

# Oxygen Reduction Electrocatalyst Based on Strongly Coupled Cobalt Oxide Nanocrystals and Carbon Nanotubes

Yongye Liang,<sup>†,⊥</sup> Hailiang Wang,<sup>†,⊥</sup> Peng Diao,<sup>†,||,⊥</sup> Wesley Chang,<sup>†</sup> Guosong Hong,<sup>†</sup> Yanguang Li,<sup>†</sup> Ming Gong,<sup>†</sup> Liming Xie,<sup>†</sup> Jigang Zhou,<sup>‡</sup> Jian Wang,<sup>‡</sup> Tom Z. Regier,<sup>‡</sup> Fei Wei,<sup>§</sup> and Hongjie Dai<sup>\*,†</sup>

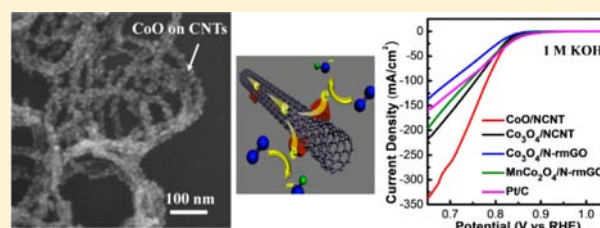
<sup>†</sup>Department of Chemistry, Stanford University, Stanford, California 94305, United States

<sup>‡</sup>Canadian Light Source Inc., Saskatoon, SK S7N 0X4, Canada

<sup>§</sup>Department of Chemical Engineering, Tsinghua University, Beijing 100084, China

## Supporting Information

**ABSTRACT:** Electrocatalyst for oxygen reduction reaction (ORR) is crucial for a variety of renewable energy applications and energy-intensive industries. The design and synthesis of highly active ORR catalysts with strong durability at low cost is extremely desirable but remains challenging. Here, we used a simple two-step method to synthesize cobalt oxide/carbon nanotube (CNT) strongly coupled hybrid as efficient ORR catalyst by directly growing nanocrystals on oxidized multiwalled CNTs. The mildly oxidized CNTs provided functional groups on the outer walls to nucleate and anchor nanocrystals, while retaining intact inner walls for highly conducting network. Cobalt oxide was in the form of CoO due to a gas-phase annealing step in NH<sub>3</sub>. The resulting CoO/nitrogen-doped CNT (NCNT) hybrid showed high ORR current density that outperformed Co<sub>3</sub>O<sub>4</sub>/graphene hybrid and commercial Pt/C catalyst at medium overpotential, mainly through a 4e<sup>-</sup> reduction pathway. The metal oxide/carbon nanotube hybrid was found to be advantageous over the graphene counterpart in terms of active sites and charge transport. Last, the CoO/NCNT hybrid showed high ORR activity and stability under a highly corrosive condition of 10 M NaOH at 80 °C, demonstrating the potential of strongly coupled inorganic/nanocarbon hybrid as a novel catalyst system in oxygen depolarized cathode for chlor-alkali electrolysis.



## INTRODUCTION

Exploring new electrocatalysts to enhance the kinetics of the otherwise sluggish oxygen reduction reaction (ORR) is important to various renewable energy applications such as fuel cells and metal-air batteries. The cathode oxygen electrocatalyst has been one of the major limiting factors for energy conversion efficiency, cost, and stability of these devices.<sup>1</sup> ORR electrocatalysts are also important to chlor-alkali electrolysis, an energy-intensive reaction that consumes an estimated ~2% electricity in the United States.<sup>2</sup> The use of oxygen depolarized cathode can save ~30% energy as compared to the hydrogen evolving cathode due to the lower cell voltage. High performance ORR catalysts are required to lower the overpotential and sustain the corrosive operating condition. To substitute the active but expensive Pt-based ORR catalyst,<sup>3</sup> low cost alternatives such as metal–N complex on carbon matrixes,<sup>4</sup> perovskites,<sup>5</sup> spinel oxides,<sup>6</sup> and doped carbonaceous materials<sup>7</sup> have been explored with promising advances.<sup>4a,c</sup> However, the current catalyst materials are still far from meeting the requirements of combined high catalytic activity, strong durability, and low cost. New strategies to develop efficient ORR catalysts are still desirable.

As relatively new classes of carbon-based nanomaterials, graphene and carbon nanotube (CNT) have high electrical conductivity, large surface area, high mechanical strength, and

structural flexibility, making them useful substrates for producing hybrid and composite materials for various applications.<sup>8</sup> In particular, due to their desirable electrical and mechanical properties, graphene and CNT could be used to derive advanced electrocatalysts.<sup>9</sup> Indeed, CNTs and graphene have been used as supports for precious metals (like Pt and Pd) to improve ORR catalytic activity and stability as compared to other carbon-based supports.<sup>10</sup> Recently, we synthesized a hybrid material of Co<sub>3</sub>O<sub>4</sub> nanocrystals grown on mildly oxidized graphene oxide (GO) that was subsequently reduced and N-doped. The resulting strongly coupled hybrid exhibited much higher ORR activity than free Co<sub>3</sub>O<sub>4</sub> nanoparticles, free GO, and their physical mixture.<sup>11</sup> The Co<sub>3</sub>O<sub>4</sub>/nitrogen-doped reduced GO (N-rmGO) hybrid catalyst outperformed commercial Pt/C catalyst (20 wt % Pt on Vulcan carbon black) in terms of stability while exhibiting high ORR activity in alkaline solutions. Through cation substitution, we further developed a MnCo<sub>2</sub>O<sub>4</sub>/N-rmGO hybrid, which outperformed Co<sub>3</sub>O<sub>4</sub>/N-rmGO and even Pt/C in ORR current density at medium overpotentials.<sup>12</sup> On the other hand, a Co<sub>1-x</sub>S/RGO hybrid material was synthesized to afford high ORR catalytic performance among all cobalt chalcogenide

Received: June 11, 2012

Published: September 8, 2012

based ORR catalysts in acidic media.<sup>13</sup> A key factor of these hybrid materials was that GO with a suitable degree of oxidation must be used for high performance catalysts because functional groups are needed for nucleating and anchoring nanocrystals on GO sheets to achieve covalent attachment. However, a dilemma is that the existence of defects and functional groups on graphene sheets could lower its electroconductivity and limit the catalytic performance of the hybrid material. We postulate that multiwalled CNT (MWCNT) or few-walled CNTs could overcome this problem as the inner graphitic walls could remain intact to provide highly conducting network while the outermost wall can be oxidized and functionalized to afford chemical reactivity, as shown recently in developing a nanotube–graphene complex for ORR in acidic conditions.<sup>14</sup> Therefore, it is highly interesting to hybridize CNTs with active nonprecious inorganic nanocrystals to afford high performance ORR catalysts.

The synthesis of CNT–inorganic nanocrystal hybrids or composites has been explored in the past decade and can be categorized by *ex situ* (attaching presynthesized nanocrystals to CNTs)<sup>15</sup> and *in situ* (synthesizing nanocrystals in the presence of CNTs) methods.<sup>8c</sup> The binding between CNT and nanocrystals could be established by noncovalent interactions (such as  $\pi$ – $\pi$  stacking and hydrophobic wrapping) or covalent bonding through functionalization of outer wall by oxidation,<sup>16</sup> cycloaddition,<sup>17</sup> or radical addition.<sup>18</sup> One method is to nucleate and grow inorganic nanocrystals on oxidized CNTs, as has been applied to the synthesis of several metal oxide/CNT hybrids such as SnO<sub>2</sub>/CNT,<sup>19</sup> RuO<sub>2</sub>/CNT,<sup>20</sup> and Co<sub>3</sub>O<sub>4</sub>/CNT.<sup>21</sup> However, little was done to control the synthesis selectively on oxidized CNTs and avoid free-growth. Also, little has been done to identify an optimal oxidation method and to control the CNT oxidation degree for maximizing interactions while maintaining the electrical properties of CNTs. Further, there are few reports on investigating the nature of coupling between inorganic nanomaterials and CNTs.

Cobalt oxide/CNT hybrids have not been investigated as ORR electrocatalysts thus far, presumably due to the low ORR activity of free cobalt oxide nanoparticles or mixture with carbon materials. It was not appreciated until recently that covalent hybridization of cobalt oxide with graphene oxide could lead to drastically improved ORR activity of Co<sub>3</sub>O<sub>4</sub>.<sup>10</sup> Here, we report the development of cobalt oxide/CNT covalent hybrid as highly efficient ORR catalyst by directly growing CoO nanocrystals on mildly oxidized MWCNTs. The hybrid was prepared by a simple two-step method including a mild solution-phase synthesis step followed by gas-phase annealing at 400 °C in a NH<sub>3</sub> atmosphere. Cobalt oxide was in the form of CoO due to thermal annealing in the reducing NH<sub>3</sub> environment. The resulting CoO/nitrogen-doped CNT (NCNT) hybrid showed much higher ORR current density than our recently reported Co<sub>3</sub>O<sub>4</sub>/N-rmGO<sup>11</sup> and MnCo<sub>2</sub>O<sub>4</sub>/N-rmGO<sup>12</sup> graphene hybrids and Co<sub>3</sub>O<sub>4</sub>/NCNT hybrid prepared by hydrothermal method at 150 °C. The CoO/NCNT catalyst also outperformed the commercial Pt/C catalyst at medium overpotentials when loaded onto Teflon-coated carbon fiber paper. Electrochemical and X-ray absorption near edge structure (XANES) spectroscopy measurements revealed strong coupling effects between cobalt oxide and CNT, favoring highly efficient charge transport in the CNT hybrid for ORR catalysis. The strongly coupled CNT

hybrid materials afforded a higher performance electrocatalyst for oxygen reduction than did the graphene counterpart.

## RESULTS AND DISCUSSION

Mildly oxidized CNT (moCNT) was first prepared using a commercial MWCNT material (FloTube 9000 from CNano Technology Ltd.). The oxidation step was important to introduce oxygen functional groups on the side walls of CNTs. A modified Hummers method<sup>22</sup> was used to prepare moCNT with controlled oxidation degree by varying the ratio of KMnO<sub>4</sub> oxidant to CNT. An optimized ratio was found to be KMnO<sub>4</sub>/CNT = 1 by mass, with the resulting oxidized CNTs containing ~20 at. % oxygen determined by X-ray photoelectron spectroscopy (XPS). Cobalt oxide/CNT hybrid was synthesized by a modified two-step method from our previous report.<sup>11,13,23</sup> In the first step, Co(OAc)<sub>2</sub> was reacted with moCNTs in an ethanol/water (15/1, volume ratio) solution at 80 °C to selectively nucleate and grow the hydrolyzed precursors on moCNTs without any free particle growth in solution. Ammonium hydroxide was added to reach a pH around 9, under which nucleation and growth of metal oxide species were highly selective on the functional groups of moCNTs. The added ammonium hydroxide was also found to provide a source of nitrogen doping of CNTs. In the second step, thermal annealing at 400 °C in a NH<sub>3</sub>/Ar atmosphere was performed to afford crystallization of the metal oxide nanoparticles and N-doped CNT, yielding the final cobalt oxide/NCNT hybrid material.

Scanning electron microscopy (SEM) and transmission electron microscopy (TEM) clearly showed the formation of nanoparticles with average size of ~5 nm on CNTs, with almost no nanoparticles detached from nanotubes (Figure 1a). The electron diffraction pattern did not match spinel Co<sub>3</sub>O<sub>4</sub>, the thermal-dynamically favored form of cobalt oxide, but matched the cubic CoO rock salt structure (Figure 1b inset). The lattice fringes of the nanoparticle from high-resolution TEM (Figure 1c) were consistent with the CoO crystal structure. High-resolution images also revealed that the

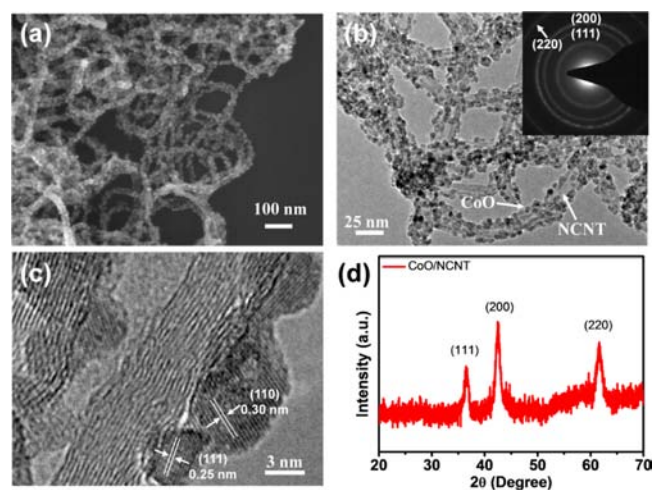


**Figure 1.** (a) Low magnification SEM and (b) TEM images of the CoO/NCNT hybrid. Inset in (b) shows an electron diffraction pattern of the hybrid. The inside circle corresponded to graphite (002) from CNT. (c) A high magnification TEM image of the CoO/NCNT hybrid. (d) A XRD spectrum of a compacted film of the CoO/NCNT hybrid.

graphitic carbon nanotube inner walls in the hybrid were undisrupted and continuous (Figure 1c), suggesting that the inner walls of CNTs were not destroyed by the oxidation and reactions during the hybrid synthesis. X-ray diffraction (XRD) further confirmed that the nanoparticles grown on carbon nanotubes were in the rock salt CoO structure (Figure 1d). The CoO phase was formed during thermal annealing at 400 °C in the reducing environment of NH<sub>3</sub> in the second step of experiment. A control experiment of hydrothermal treatment at 150 °C in the second step yielded hybrid material with similar morphology, but the nanoparticles were in spinel Co<sub>3</sub>O<sub>4</sub> structure (Figure S1). XPS revealed composition differences between CoO and Co<sub>3</sub>O<sub>4</sub> hybrids in Co to O ratio (Figure 2).

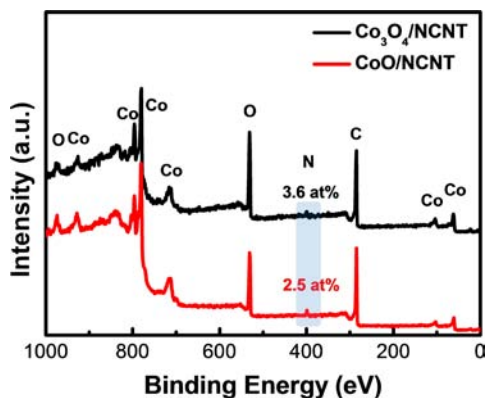


**Figure 2.** XPS spectra of the CoO/NCNT and Co<sub>3</sub>O<sub>4</sub>/NCNT hybrids.

N doping was detected in both hybrids with the CoO/NCNT showing lower N percentage (~3.6 at. % for Co<sub>3</sub>O<sub>4</sub>/NCNT and ~2.5 at. % for CoO/NCNT). The high temperature annealing could have removed some labile N functional group in the CoO/NCNT hybrid. It was found that the hybrid contained ~67 wt % CoO oxide by thermal-gravimetric analysis.

The ORR catalytic activity of the CoO/NCNT hybrid was first evaluated by cyclic voltammetry (CV). The CoO/NCNT hybrid showed an ORR onset potential of 0.93 V and a peak potential of 0.86 V vs the reversible hydrogen electrode (RHE) in 1 M KOH, which were much more positive than those of the pure NCNT control (made by the same method but without any Co species added) (Figure 3a). The higher activity in the hybrid was also gleaned from the higher peak current density. Both the ORR onset and the peak potentials of the CoO/NCNT hybrid were similar to those of the hydrothermally derived Co<sub>3</sub>O<sub>4</sub>/NCNT and Co<sub>3</sub>O<sub>4</sub>/N-rmGO hybrids (Figure 3b). Rotating disk electrode (RDE) measurements found that the three hybrids exhibited very similar linear sweep voltammograms with similar half-wave potential, about 35 mV more negative than Pt/C catalyst (Figure 3c). These indicated that CoO/NCNT, Co<sub>3</sub>O<sub>4</sub>/NCNT, and Co<sub>3</sub>O<sub>4</sub>/N-rmGO contained similar active sites in nature for ORR. However, the CoO/NCNT hybrid afforded higher peak current density by ~30% than the other two hybrids in CVs, suggesting that the CoO/NCNT hybrid material contained a larger number of effective or accessible ORR active sites.

We recorded cyclic voltammograms in N<sub>2</sub> saturated 1 M KOH with freshly made and stored CoO/NCNT and Co<sub>3</sub>O<sub>4</sub>/NCNT hybrids (Figure 3d). All of the hybrids showed similar

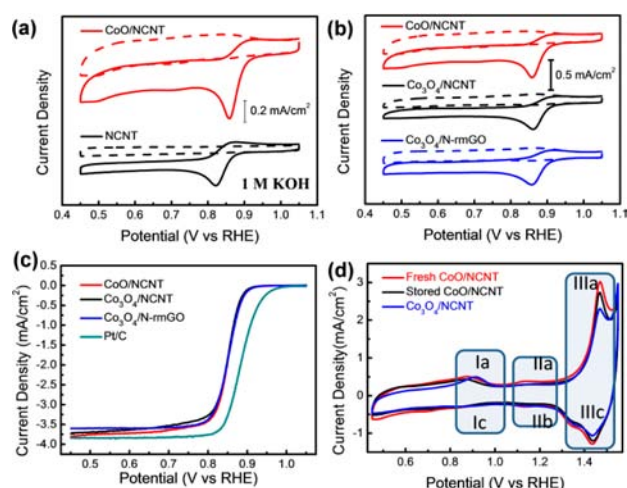
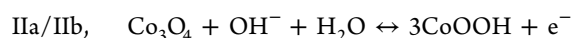
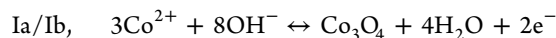


**Figure 3.** (a) CV curves of the CoO/NCNT hybrid and NCNT on glassy carbon electrodes in O<sub>2</sub>-saturated (solid line) and N<sub>2</sub>-saturated (dash line) 1 M KOH. (b) CV curves of the CoO/NCNT, Co<sub>3</sub>O<sub>4</sub>/NCNT, and Co<sub>3</sub>O<sub>4</sub>/N-rmGO hybrids on glassy carbon electrodes in O<sub>2</sub>-saturated (solid line) or N<sub>2</sub>-saturated (dash line) 1 M KOH. (c) Rotating-disk electrode voltammograms of the CoO/NCNT, Co<sub>3</sub>O<sub>4</sub>/NCNT, Co<sub>3</sub>O<sub>4</sub>/N-rmGO, and Pt/C in O<sub>2</sub>-saturated 1 M KOH with a sweep rate of 5 mV/s at 1600 rpm. (d) Typical CV response of freshly made CoO/NCNT, stored CoO/NCNT and Co<sub>3</sub>O<sub>4</sub>/NCNT hybrids in N<sub>2</sub>-saturated 1 M KOH. Scan rate was 20 mV/s. Catalyst loading was 0.10 mg/cm<sup>2</sup> for all samples.

electrochemical behaviors, and the three sets of redox couples could be assigned to:<sup>24</sup>



The oxidation state of Co species was determined by the range of potential scan for both the CoO/NCNT hybrid and the Co<sub>3</sub>O<sub>4</sub>/NCNT hybrid. The CoO/NCNT hybrid (stored in air >1 day, general sample used in the paper) and Co<sub>3</sub>O<sub>4</sub>/NCNT hybrids did not show an obvious IIa peak in the voltammograms. Interestingly, freshly made CoO/NCNT hybrid (stored <1 day) showed a more obvious IIa peak. Co<sub>3</sub>O<sub>4</sub> did not show an obvious IIa peak as a CoOOH surface layer was spontaneously formed when Co<sub>3</sub>O<sub>4</sub> was in contact with an alkaline electrolyte.<sup>25</sup> This result indicated that the surface of CoO nanoparticle in the hybrid was oxidized to Co<sub>3</sub>O<sub>4</sub> when stored in air. Both freshly made and stored CoO/NCNT showed a more negative Ia peak than Co<sub>3</sub>O<sub>4</sub>/NCNT hybrid, suggesting that the unoxidized part of the CoO nanoparticle possibly made the CoO/NCNT hybrids more electron rich than the Co<sub>3</sub>O<sub>4</sub>/NCNT hybrid.<sup>26</sup>

The ORR pathways catalyzed by the CoO/NCNT hybrid were investigated by rotating ring-disk electrode (RRDE) measurements. At a rotating rate of 1600 rpm in 1 M KOH, the disk current from oxygen reduction was much larger than the ring current from peroxide oxidation in the CoO/NCNT hybrid (Figure 4a). The hybrid gave higher disk current and lower ring current than the NCNT control, suggesting higher ORR catalytic activity of the hybrid. The calculated peroxide yield from the RRDE data was less than 12% for the CoO/NCNT hybrid over the range from 0.9 to 0.45 V vs RHE, while it was higher than 35% for NCNT (Figure 4b). The average

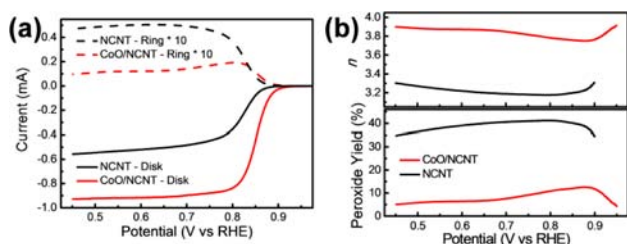


**Figure 4.** (a) Rotating ring-disk electrode voltammogram of CoO/NCNT hybrid and NCNT in  $O_2$ -saturated 1 M KOH at 1600 rpm. The disk potential was scanned at 5 mV/s, and the ring potential was constant at 1.3 V vs RHE. (b) Peroxide yield (bottom) and the electron transfer number ( $n$ ) (top) of the CoO/NCNT hybrid and NCNT at various potentials based on the corresponding RRDE data in (a). Catalyst loading was 0.10 mg/cm<sup>2</sup> for all samples.

electron transfer number ( $n$ ) is about 3.9 for CoO/NCNT hybrid and about 3.3 for NCNT (Figure 4b). The hydrothermally synthesized  $Co_3O_4$ /NCNT hybrid showed a performance similar to that of the CoO/NCNT hybrid in the RRDE measurement (Figure S2), suggesting both of these NCNT hybrids favored a 4-electron reduction pathway for ORR.

To investigate the ORR catalytic properties of our catalyst in a setting close to practical fuel cell operation, we loaded the catalysts on Teflon-coated carbon fiber paper (TCFP) (at a loading of  $\sim 0.24$  mg/cm<sup>2</sup>) to measure  $iR$ -compensated polarization curves.<sup>11,12</sup> The porous TCFP substrate is highly hydrophobic, providing a three-phase contact point for oxygen, electrolyte, and catalyst. Therefore, the measured current on TCFP is not as limited by oxygen concentration in the electrolyte as on other substrates and can reflect the kinetic property of the catalyst loaded. The hydrothermally derived  $Co_3O_4$ /NCNT exhibited significantly higher ORR current density than the  $Co_3O_4$ /N-rmGO hybrid (Figure 5a). Even though the  $Co_3O_4$ /NCNT hybrid had a lower BET surface area than  $Co_3O_4$ /N-rmGO (the BET surface area is 210 m<sup>2</sup>/g for  $Co_3O_4$ /N-rmGO and 154 m<sup>2</sup>/g for  $Co_3O_4$ /NCNT, respectively), it was possible that the higher electrical conductivity of mCNT than that of N-rmGO made MWCNT a higher performance substrate to form hybrids for ORR electrocatalysis. The electrical resistance measured from a pellet of  $Co_3O_4$ /NCNT hybrid ( $\sim 40$ – $60$   $\Omega$ ) was much smaller than that of  $Co_3O_4$ /N-rmGO hybrid ( $\sim 200$ – $300$   $\Omega$ ) (see Experimental Section for details), which could account for the higher ORR current density afforded by the  $Co_3O_4$ /NCNT hybrid.

At the same catalyst loading on TCFP (0.24 mg/cm<sup>2</sup>), the gas-phase derived CoO/NCNT hybrid showed much higher ORR current density than did the hydrothermal  $Co_3O_4$ /NCNT hybrid. It also outperformed the commercial Pt/C catalyst and a high performance  $MnCo_2O_4$ /N-rmGO hybrid reported recently<sup>12</sup> at potential  $< 0.80$  V vs RHE in 1 M KOH (Figure 3a). At 0.7 V, the CoO/NCNT hybrid afforded an ORR current density more than 2 times that of Pt/C (266 mA/cm<sup>2</sup> for CoO/NCNT vs 124 mA/cm<sup>2</sup> for Pt/C). Each component alone (CoO or NCNT) and their physical mixture (CoO + NCNT) showed significantly lower current densities than the CoO/NCNT hybrid (Figure 5b). Although the NCNT alone showed certain ORR activity, the direct contribution of NCNT to the ORR current in the hybrid was small considering the lower activity and only 33 wt % NCNT in the hybrid. These

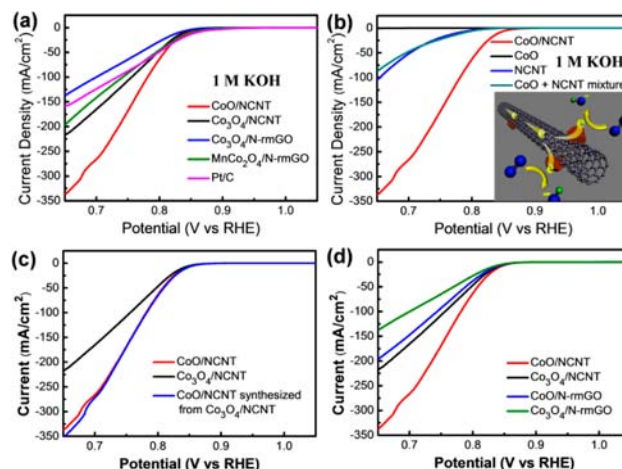


**Figure 5.** Oxygen reduction polarization curves recorded with (a) the CoO/NCNT hybrid, hydrothermally derived  $Co_3O_4$ /NCNT hybrid, and  $Co_3O_4$ /N-rmGO hybrid,<sup>11</sup>  $MnCo_2O_4$ /N-rmGO hybrid,<sup>12</sup> and Pt/C catalyst; (b) the CoO/NCNT hybrid, free CoO nanoparticles, NCNT and CoO + NCNT physical mixture; inset in (b) shows a cartoon of CoO/NCNT hybrid for oxygen reduction catalysis; (c) the CoO/NCNT hybrid prepared from hydrothermally treated  $Co_3O_4$ /NCNT, the initial  $Co_3O_4$ /NCNT hybrid, and CoO/NCNT hybrid; and (d) the CoO/NCNT and CoO/N-rmGO hybrids prepared by thermal annealing in  $NH_3$  and the  $Co_3O_4$ /NCNT and  $Co_3O_4$ /N-rmGO hybrids prepared by hydrothermal treatment. All of the samples were loaded on carbon fiber paper with  $\sim 0.24$  mg/cm<sup>2</sup> and measured in 1 M KOH.

results suggested that the high performance of the CoO/NCNT hybrid material was a result of collective action by the CoO and NCNT in the hybrid as a whole (Figure 5b, inset).

We found that the hydrothermally prepared  $Co_3O_4$ /NCNT hybrid showed the same ORR current density as the CoO/NCNT hybrid after  $NH_3$  thermal annealing at 400  $^{\circ}C$  (Figure 5c), suggesting that the annealing step was important to optimize the ORR activity of cobalt oxide and nanotube hybrid. Annealing of  $Co_3O_4$ /NCNT in  $NH_3$  led to a slight decrease of electrical resistance ( $\sim 20$ – $30$   $\Omega$  vs  $\sim 40$ – $60$   $\Omega$  in the original  $Co_3O_4$ /NCNT hybrid) and conversion of  $Co_3O_4$  to CoO. A CoO/N-rmGO hybrid prepared by 400  $^{\circ}C$  gas-phase annealing in  $NH_3$  of  $Co_3O_4$ /N-rmGO made hydrothermally<sup>11</sup> also exhibited improved ORR current density than the hydrothermally synthesized  $Co_3O_4$ /N-rmGO hybrid reported in ref 10, although it was still below the performance of the CoO/NCNT hybrid (Figure 5d). This result confirmed that  $NH_3$  annealing was general to improve the ORR performance of cobalt oxide/CNT and cobalt oxide/graphene hybrid materials.

We performed electrochemical impedance spectroscopy measurements in the ORR region at 0.8 V for various catalysts. The Nyquist plots revealed that CoO/NCNT hybrid exhibited the smallest charge transfer resistance as compared to Pt/C,  $Co_3O_4$ /NCNT, and NCNT (Figure 6a). The CoO/NCNT hybrid was the most effective in shuttling charges from electrode to oxygen, improving ORR catalysis. The  $Co_3O_4$ /NCNT hybrid showed a smaller semicircle than did the  $Co_3O_4$ /N-rmGO hybrid in the Nyquist plots at 0.8 V (Figure S3), suggesting a smaller charge transfer resistance in the NCNT hybrid material during ORR, likely due to the higher electrical conductivity of the NCNT hybrid than the N-rmGO hybrid. Besides the high activity, the CoO/NCNT hybrid also exhibited excellent stability as measured by chronoamperometry.

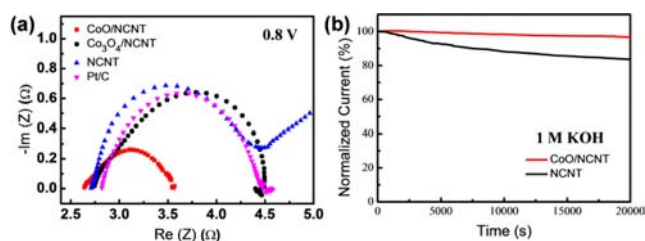


**Figure 6.** (a) Impedance data of the CoO/NCNT, Co<sub>3</sub>O<sub>4</sub>/NCNT hybrids, NCNT, and Pt/C at 0.8 V vs RHE. (b) Chronoamperometric responses of the CoO/NCNT hybrid and NCNT on carbon fiber paper electrodes kept at 0.70 V vs RHE in O<sub>2</sub>-saturated 1 M KOH. Catalyst loading was  $\sim 0.24$  mg/cm<sup>2</sup> for all samples.

metric measurements. At a constant voltage of 0.70 V vs RHE, the ORR current density produced in the hybrid catalyst decreased by less than 4% over 5.5 h of continuous operation, while the pure NCNT catalyst exhibited  $\sim 18\%$  decrease in current density (Figure 6b).

X-ray absorption near-edge structure (XANES) measurements were employed to glean nanoparticle structures and the interactions between metal oxide and CNT in the CoO/NCNT hybrid. The Co-L edge absorption of the hybrid matched the octahedrally coordinated Co<sup>2+</sup> state (Figure 7a), consistent

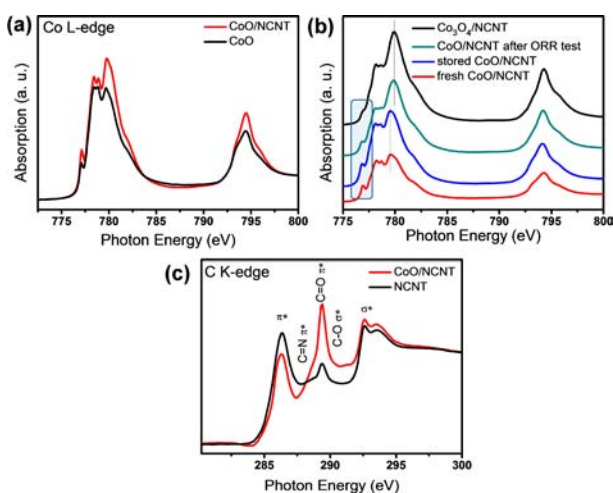


**Figure 7.** (a) Co L-edge XANES of the CoO/NCNT hybrid (red curve) and free CoO nanoparticles (black curve). (b) Co L-edge XANES of the stored CoO/NCNT hybrid loaded on carbon fiber paper before (blue curve) and after (green curve) ORR cycling. The spectra of fresh CoO/NCNT hybrid (red curve) and Co<sub>3</sub>O<sub>4</sub>/NCNT hybrid (black curve) were also shown for comparison. (c) Carbon K-edge XANES of the CoO/NCNT hybrid (red curve) and NCNT (black curve).

with the rock salt CoO structure.<sup>27</sup> The CoO/NCNT hybrid stored in air for 2 months showed slightly enhanced absorption in the high energy region of Co L-edge as compared to freshly made sample (Figure 7b), suggesting surface oxidation of the CoO nanoparticles. We also measured the Co-L edge of CoO/NCNT hybrid after ORR cycling test between 1.0 and 0.4 V vs RHE for 2000 cycles. We observed an increase in the ratio of the high energy peak ( $\sim 779.7$  eV) intensity to low energy peak ( $\sim 778.6$  eV) intensity, and a shift of the high energy peak toward the Co-L edge of the Co<sub>3</sub>O<sub>4</sub> hybrid<sup>28</sup> (Figure 7b). This result indicated oxidation of CoO to Co<sub>3</sub>O<sub>4</sub> through ORR catalysis in KOH. However, both the persistence of the

absorption peak at 777.0 eV and the lower ratio of the high energy peak intensity to low energy peak intensity than that in Co<sub>3</sub>O<sub>4</sub> at the Co-L edge suggested partial retention of the CoO structure (Figure 7b). Because 50% of the XANES signal was from the top  $\sim 1$  nm on the sample surface,<sup>29</sup> the conversion of CoO to Co<sub>3</sub>O<sub>4</sub> likely occurred on the surface of the nanoparticles. Electron diffraction patterns of the CoO/NCNT hybrid after ORR test measurements also confirmed the existence of CoO and Co<sub>3</sub>O<sub>4</sub> phases in the hybrid (Figure S4).

At the carbon K-edge, the CoO/NCNT hybrid showed a significant increase in the peak absorption intensity around  $\sim 289.3$  eV as compared to NCNT control (Figure 7c), which was attributed to the C–O, C–N functional groups on CNT.<sup>30</sup> This suggested possible formation of Co–O–C and Co–N–C bonds in the hybrid material. A lower adsorption intensity of the  $\pi^*$  peak of  $\sim 286.3$  eV at the C–K edge of the hybrid as compared to the NCNT control and higher adsorption intensity at the Co-L edge of the CoO/NCNT hybrid sample as compared to CoO were observed (Figure 7c and a), suggesting possible electron transfer from Co to CNT in the hybrid material.<sup>31</sup> The bond formations and charge transfer indicated the intimate couplings between CoO nanoparticles and NCNT. The nitrogen K-edge spectrum of the CoO/NCNT hybrid confirmed the N-doping in the hybrid (Figure S5). The perturbation of N K-edge XANES of the hybrid as compared to NCNT may suggest the interaction of CoO nanoparticle with N on NCNT.

It has been proposed that “Co–N<sub>x</sub>” could be a possible ORR active site in some catalyst systems.<sup>32</sup> Such an active site could contribute to the ORR performance of the CoO/NCNT hybrid. However, we suggest that the main active site in our hybrid system may differ from the “Co–N<sub>x</sub>” site based on that the CoOx/CNT hybrid without any N doping (prepared without NH<sub>4</sub>OH addition in the first step and annealing in Ar without NH<sub>3</sub> in second step) showed ORR onset potential (0.91 V) and peak potential (0.83 V) similar to those of the CoO/NCNT hybrid (onset 0.93 V and peak 0.86 V) (Figure 8). This suggests cobalt oxide responsible for high ORR activity in both hybrids. This was further consistent with the fact that our hybrids had much higher Co content than most of the “Co–N<sub>x</sub>” catalysts. The optimal Co loading in the CoO/NCNT hybrid for high ORR activity was  $\sim 12$ –20 at. %

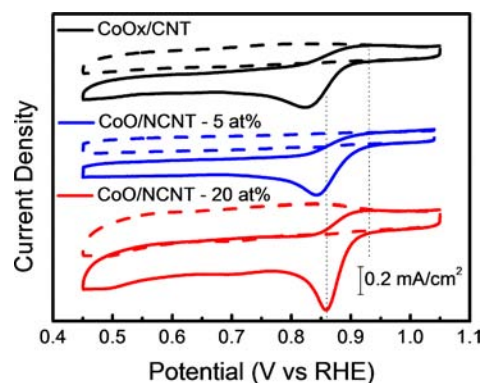


**Figure 8.** CV curves of the CoOx/CNT hybrid and the CoO/NCNT hybrid with 5 and 20 at. % Co loading on glassy carbon electrodes in O<sub>2</sub>-saturated (solid line) or N<sub>2</sub>-saturated (dash line) 1 M KOH. Catalyst loading was 0.10 mg/cm<sup>2</sup> for all samples.

(corresponding to ~50–67 wt % CoO), while the optimal Co loading in most of the “Co–N<sub>x</sub>” systems was less than 5 at. %.<sup>32a,b</sup> The CoO/NCNT hybrid made with 5 at. % Co showed substantially smaller peak current density as compared to the hybrid with 20 at. % Co in CV with the same mass loading (Figure 8). A portion of Co from the CoO nanoparticle may interact with nitrogen on carbon nanotube to form intimate bonding, facilitating charge transfer between CNT and nanoparticle, and affording improvement in ORR activity of the N-doped hybrid.

We used CNTs oxidized to different degrees for preparing CoO/NCNT hybrids and compared their ORR performances (Figure 9a). CNTs were oxidized by varying the KMnO<sub>4</sub>/CNT

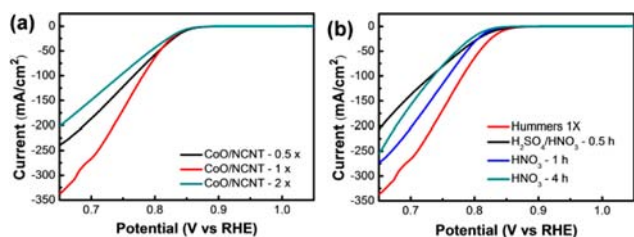


**Figure 9.** (a) Oxygen reduction polarization curves of the CoO/NCNT hybrids prepared by oxidized CNT with different oxidation degree. (b) Oxygen reduction currents of the CoO/NCNT hybrids prepared from CNT with different oxidation method. Catalyst loading was ~0.24 mg/cm<sup>2</sup> for all samples.

ratio. It was found that the CoO/NCNT hybrid made by 1X moCNT (KMnO<sub>4</sub>/CNT = 1, mass ratio) afforded higher performance than hybrids derived from 0.5X and 2X moCNTs. The result indicated that controlling CNT oxidation was important to optimize activity of the CoO/CNT hybrid material, likely due to the existence of a balance between electrical conductivity and density of functional groups on CNTs. Strong oxidizing acids (like HNO<sub>3</sub> and HNO<sub>3</sub>–H<sub>2</sub>SO<sub>4</sub>) are commonly used to oxidize CNT for preparation of hybrid materials.<sup>8c,16</sup> As a control, we oxidized the same MWCNTs by refluxing in HNO<sub>3</sub>–H<sub>2</sub>SO<sub>4</sub> (3/1, volume ratio) for 0.5 h and obtained oxCNTs with a high oxidation degree (>36% oxygen). The CoO hybrid made from such oxCNT exhibited only one-half of the ORR current density of the hybrid prepared from Hummers 1X moCNT (Figure 9b), possibly due to the overoxidation of CNT and loss of electrical conductivity. Milder oxidized MWCNTs were prepared by refluxing in HNO<sub>3</sub> for 1 and 4 h with lower oxygen content of 9% and 15%, respectively. Their corresponding CoO hybrids also exhibited lower catalytic activities than that of Hummers 1X moCNT (Figure 9b). XPS measurements revealed that the Hummers 1X moCNT had a higher ratio of –COO species to C–O species (9%/21%) than that of oxCNT prepared by refluxing in HNO<sub>3</sub> for 4 h (6%/26%), suggesting that the Hummers oxidizing method was advantageous in producing more abundant –COO species that could serve as nucleation and anchored sites for nanocrystal growth on oxidized CNTs. This highlighted the importance of oxidation method for the synthesis of inorganic/nanocarbon hybrids.

Hybrid materials prepared by thermal annealing in argon were also investigated. The CoO<sub>x</sub>/NCNT hybrid annealed at 400 °C in Ar showed lower ORR current density than the CoO/NCNT hybrid prepared by NH<sub>3</sub> annealing at 400 °C (Figure S6). Although the Ar annealed hybrid had morphology similar to that of the NH<sub>3</sub> annealed CoO/NCNT hybrid

(Figure S7a), the oxide nanoparticles were found to be mixtures of CoO and Co<sub>3</sub>O<sub>4</sub> in Ar annealed hybrid (Figure S7b). This suggested that cobalt oxide hybrid was less reduced in Ar atmosphere at 400 °C, which led to the incomplete conversion of Co<sub>3</sub>O<sub>4</sub> to CoO and lower degree of reduction of moCNT as well. Both could be factors for the lower performance of the Ar annealed hybrid at 400 °C. Further raising the Ar annealing temperature to 650 °C yielded hybrid material with higher ORR current density close to the NH<sub>3</sub> annealed CoO/NCNT hybrid (Figure S6). The result indicated that better reduction at high temperature by thermal annealing, especially in the presence of NH<sub>3</sub>, improved the ORR performance of the hybrid material.

The effect of CoO loading percentage in the CoO/NCNT hybrid to the ORR catalytic performance was also investigated. Hybrids with different CoO mass percentages were synthesized by varying the Co(OAc)<sub>2</sub>/moCNT ratio in the first step. From measurements on carbon fiber paper, we found that the optimum CoO content was in the range between ~50% and ~67% by mass (Figure S8). The optimal nanoparticle content in CNT hybrid was smaller than that of our previously reported graphene hybrid<sup>12</sup> due to the lower surface area of CNT than graphene. Higher CoO content than this range could cause free growth of CoO nanoparticles, while lower CoO content could make fewer catalytic sites for ORR, both leading to the decrease of catalytic performance for ORR.

Last, we investigated the catalytic performance of our CoO/NCNT hybrid material under a harsh condition of 10 M NaOH at 80 °C (see Experimental Section), which is a standard condition employed in oxygen depolarized cathode for chlor-alkali electrolysis.<sup>2</sup> The CoO/NCNT hybrid exhibited excellent ORR catalytic activity in 10 M NaOH at 80 °C and afforded higher ORR current than Pt/C at potential voltages < ~–0.15 V vs the Hg/HgO reference electrode (MMOE) for the same mass loading (~0.48 mg/cm<sup>2</sup>) (Figure 10a). High stability was

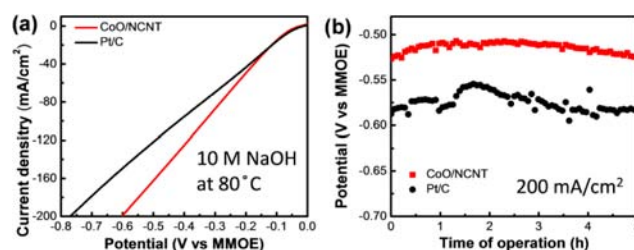


**Figure 10.** Electrochemical performance of the CoO/NCNT hybrid and Pt/C in 10 M NaOH at 80 °C. (a) Oxygen reduction polarization curves without *iR* compensation of the CoO/NCNT hybrid and Pt/C; and (b) potential versus time response of the oxygen cathode catalyzed by the CoO/NCNT hybrid and Pt/C at 200 mA/cm<sup>2</sup>. Catalyst loading is ~0.48 mg/cm<sup>2</sup> for all samples.

also a major feature of the CoO/NCNT hybrid under the chlor-alkali condition (Figure 10b). No significant increase in the cathode potential was observed during continuous ORR operation for 5 h at a constant, high current density of 200 mA/cm<sup>2</sup> (~400 mA/mg). Impressively, the CoO/NCNT hybrid afforded lower overpotential than the Pt/C through the identical chronopotentialmetric measurements (Figure 10b), suggesting that the CoO/NCNT hybrid is a highly promising electrocatalyst for ORR in chlor-alkali electrolysis.

## CONCLUSION

We developed a simple two-step method to synthesize a CoO/NCNT hybrid by growing nanocrystals on mildly oxidized carbon nanotubes. The hybrid synthesis was well controlled to achieve selective nucleation on oxidized CNTs, and the CNT oxidation degree was well balanced to afford intimate coupling between the nanocrystals and carbon nanotubes without destroying the electrical properties of the CNTs. The higher ORR performance than the graphene hybrid counterpart was attributed to the high electrical conductivity of the CNT hybrids due to the intact inner walls of CNTs. The CoO phase generated by NH<sub>3</sub> thermal annealing may also facilitate charge transfer to enhance the ORR catalytic activity. Thus, the CoO/CNT hybrid structure is advantageous over the graphene counterpart<sup>10</sup> in both charge transport and active catalytic sites. Because of the simple synthesis and high performance, the strongly coupled inorganic/nanocarbon hybrid, like CoO/NCNT, represents a promising alternative to Pt for ORR catalysis in renewable energy applications under alkaline conditions. The excellent activity and stability of the hybrid material under highly corrosive alkaline conditions also make it promising for chlor-alkali electrolysis.

## EXPERIMENTAL SECTION

**1. Synthesis.** *a. Synthesis of Mildly Oxidized Carbon Nanotubes (moCNT).* The mildly oxidized CNTs were made by a modified Hummers method. Multiwall CNT (MWCNT) (FloTube 9000 from CNano Technology Ltd.) was first purified by calcinations at 500 °C for 1 h and washing with dilute hydrochloric acid (10%). The purified MWCNT (1 g) was put into a 250 mL round-bottom flask. Twenty-three milliliters of concentrated sulfuric acid was added, and the mixture was stirred at room temperature overnight. Next, the flask was heated in an oil bath at 40 °C, and 200 mg of NaNO<sub>3</sub> was added to the suspension and allowed to dissolve for 5 min. This step was followed by the slow addition of 1 g of KMnO<sub>4</sub>, keeping the reaction temperature below 45 °C. The solution was allowed to stir for 30 min. Afterward, 3 mL of water was added to the flask, followed by another 3 mL after 5 min. After another 5 min, 40 mL of water was added. Fifteen minutes later, the flask was removed from the oil bath, and 140 mL of water and 10 mL of 30% H<sub>2</sub>O<sub>2</sub> were added to end the reaction. This suspension was stirred at room temperature for 5 min. It was then repeatedly centrifuged and washed with 5% HCl solution twice, followed by rinsing with copious amounts of water. The final precipitate was dispersed in 10 mL of water and lyophilized. Finally, a dry product of ~1 g was collected.

Acid oxidized CNTs were prepared by refluxing the MWCNT (500 mg) in 20 mL of acid at ~110 °C for certain time. After refluxing, the reaction was cooled to room temperature and diluted with 100 mL of water. The precipitate was collected by centrifugation and washed with water several times. The final precipitate was dispersed in 10 mL of water and lyophilized to get the dry product.

*b. Synthesis of CoO/NCNT Hybrids, NCNT, and CoO Nanoparticles.* In a typical reaction, oxCNT (18 mg) was dispersed in 24 mL of ethanol (EtOH) and 0.5 mL of water. Next, 0.6 mL of 0.6 M Co(OAc)<sub>2</sub> aqueous solution was added to the oxCNT EtOH suspension, followed by the addition of 0.5 mL of NH<sub>4</sub>OH at room temperature. The reaction was kept at 80 °C with stirring for 20 h. After that, the resulting precursor from the first step was collected by centrifugation, washed with ethanol and water, and dried by lyophilization. The powder was annealed at 400 °C for 3 h at NH<sub>3</sub>/Ar atmosphere. The final product was ~40 mg.

NCNT was made through the same steps as CoO/NCNT hybrid without adding any Co salt in the first step. Free CoO nanoparticles were made through the same steps as making CoO/NCNT without adding any moCNT in the first step.

*c. Synthesis of Co<sub>3</sub>O<sub>4</sub>/NCNT Hybrids.* oxCNT (18 mg) was dispersed in 24 mL of ethanol (EtOH) and 0.5 mL of water. Next, 0.6

mL of 0.6 M Co(OAc)<sub>2</sub> aqueous solution was added to the oxCNT EtOH suspension, followed by the addition of 0.5 mL of NH<sub>4</sub>OH at room temperature. The reaction was kept at 80 °C with stirring for 20 h. After that, the reaction mixture from the first step was transferred to a 40 mL autoclave for hydrothermal reaction at 150 °C for 3 h. The resulting product was collected by centrifugation and washed with ethanol and water. The Co<sub>3</sub>O<sub>4</sub>/NCNT hybrid product was ~38 mg after lyophilization.

**2. Sample Preparation for Characterizations.** SEM samples were prepared onto silicon substrates by drop-drying the samples from their aqueous suspensions. TEM samples were prepared by drop-drying the samples from their diluted aqueous suspensions onto copper grids. XRD samples were prepared by drop-drying the samples from their aqueous suspensions to form thick films on glass slides. Surface area of the samples was measured by Brunauer–Emmett–Teller (BET) nitrogen adsorption–desorption isotherms at 77 K with Micromeritics ASAP 2020 instrument.

**3. Electrochemical Measurements.** *a. Cyclic Voltammetry (CV) and Rotating Disk Electrode (RDE) Measurement.* The working electrode was prepared by loading catalyst sample film of 0.10 mg/cm<sup>2</sup> on glass carbon electrode. First, the ink was prepared by dispersing 4 mg of catalyst and 17 μL of 5 wt % Nafion solution (20 wt % of Nafion to catalyst ratio) in 1 mL of 2.5:1 v/v water/iso-propanol mixed solvent by at least 30 min sonication to form a homogeneous dispersion. Pt/C ink was prepared by dispersing 4 mg of Pt/C (20 wt % Pt on Vulcan XC-72) in 1 mL of EtOH with 35 μL of 5 wt % Nafion solution (40 wt % of Nafion to catalyst ratio). Next, 5 μL of the catalyst ink (containing 20 μg of catalyst) was loaded onto a glassy carbon electrode of 5 mm in diameter (loading ~0.10 mg/cm<sup>2</sup>). The ink was dried slowly in air, and the drying condition was adjusted by trial and error until a uniform catalyst distribution across the electrode surface was obtained. CV and RDE were conducted with a CHI 760 D potentiostat in a three-electrode electrochemical cell using a saturated calomel electrode as the reference electrode, and a graphite rod as the counter electrode. Electrolyte was saturated with oxygen by bubbling O<sub>2</sub> prior to the start of each experiment. A flow of O<sub>2</sub> was maintained over the electrolyte during the recording of CVs to ensure its continued O<sub>2</sub> saturation. The working electrode was cycled at least 10 times before data were recorded at a scan rate of 5 mV/s. In control experiments, CV and RDE measurements were also performed in N<sub>2</sub> by switching to N<sub>2</sub> flow through the electrochemical cell.

*b. Rotating Ring-Disk Electrode (RRDE) Measurement.* Catalyst inks and electrodes were prepared by the same method as above. The disk electrode was scanned cathodically at a rate of 5 mV/s, and the ring potential was constant at 1.3 V vs RHE. The % HO<sub>2</sub><sup>-</sup> and the electron transfer number (*n*) were determined by the following equations:<sup>33</sup>

$$\%(\text{HO}_2^-) = 200 \times \frac{I_r/N}{I_d + I_r/N}$$

$$n = 4 \times \frac{I_d}{I_d + I_r/N}$$

where *I*<sub>d</sub> is disk current, *I*<sub>r</sub> is ring current, and *N* is current collection efficiency of the Pt ring. *N* was determined to be 0.40 from the reduction of K<sub>3</sub>Fe[CN]<sub>6</sub>.

*c. Oxygen Electrode Activities on Teflon-Coated Carbon Fiber Paper.* For measurements on Teflon-coated carbon fiber paper at room temperature in 1 M KOH, the working electrode was prepared by loading ~0.24 mg of catalyst (for hybrid catalysts and Pt/C) on 1 cm<sup>2</sup> Teflon-coated carbon fiber paper (AvCarb P75T, Fuel Cell Store) from its 1 mg/mL ethanol dispersion with 10 wt % Nafion. It was cycled at least 20 times between 0 and -0.6 V vs SCE before data were recorded at a scan rate of 5 mV/s for ORR measurement. A continuous oxygen flow was supplied to the measurement setup at ~1 atm. All of the room temperature data from carbon fiber paper were *iR*-compensated.

For measurements in 10 M NaOH at 80 °C, the working electrode was prepared by loading ~0.48 mg of catalyst (for hybrid catalysts and

Pt/C) on 1 cm<sup>2</sup> Teflon-coated carbon fiber paper. To avoid the flooding problem, the substrates were placed at the electrolyte/gas interface with nickel foam support. The measurement setup was immersed in an oil bath to maintain the temperature at 80 °C during measurement, and a continuous oxygen flow was supplied at ~1 atm. Hg/HgO electrode (MMOE) was used as the reference electrode, and a graphite rod was used as the counter electrode. The analysis of polarized currents was capacitance-corrected by taking the average between negative and positive-going scans.

**d. RHE Calibration.** The saturated calomel electrode (SCE) used as the reference electrode was calibrated with respect to reversible hydrogen electrode (RHE). The calibration was performed in the high-purity hydrogen saturated electrolyte with a Pt wire as the working electrode. CVs were run at a scan rate of 1 mV/s, and the average of the two potentials at which the current crossed zero was taken to be the thermodynamic potential for the hydrogen electrode reactions. In 1 M KOH,  $E(\text{RHE}) = E(\text{SCE}) + 1.051 \text{ V}$ .

**4. Electrical Resistance Measurement.** Samples (~50 mg) were first compressed into pellets with circular surface of 0.38 cm<sup>2</sup> and thickness of ~0.7–0.8 mm. The electrical resistance of the sample was measured by multimeter with the probes applied to two sides of the pellet along the circular diameter.

**5. XANES Measurements.** XANES measurements were performed at the SGM beamline of the Canadian Light Source. Powder samples were held by indium foil. XANES were recorded in the surface sensitive total electron yield (TEY) with use of specimen current. Data were first normalized to the incident photon flux  $I_0$  measured with a refreshed gold mesh at SGM prior to the measurement. After background correction, the XANES are then normalized to the edge jump, the difference in absorption coefficient just below and at a flat region above the edge (300, 415, and 805 eV for C, N, and Co, respectively).

## ■ ASSOCIATED CONTENT

### ● Supporting Information

Supplementary figures S1–S8. This material is available free of charge via the Internet at <http://pubs.acs.org>.

## ■ AUTHOR INFORMATION

### Corresponding Author

hdai@stanford.edu

### Present Address

<sup>||</sup>School of Materials Science and Engineering, Beihang University, Beijing 100191, China.

### Author Contributions

<sup>†</sup>These authors contributed equally.

### Notes

The authors declare no competing financial interest.

## ■ ACKNOWLEDGMENTS

This work was supported by a Stinehart Grant for Energy Research at Stanford from the Stanford Precourt Institute for Energy. CLS is supported by the NSERC, NRC, CIHR of Canada, the Province of Saskatchewan, WEDC, and the University of Saskatchewan.

## ■ REFERENCES

- (1) Gewirth, A. A.; Thorum, M. S. *Inorg. Chem.* **2010**, *49*, 3557–3566.
- (2) Moussallem, I.; Joerissen, J.; Kunz, U.; Pinnow, S.; Turek, T. J. *Appl. Electrochem.* **2008**, *38*, 1177–1194.
- (3) Morozan, A.; Jousselme, B.; Palacin, S. *Energy Environ. Sci.* **2011**, *4*, 1238–1254.
- (4) (a) Lefevre, M.; Proietti, E.; Jaouen, F.; Dodelet, J.-P. *Science (Washington, DC, U.S.)* **2009**, *324*, 71–74. (b) Meng, H.; Jaouen, F.; Proietti, E.; Lefevre, M.; Dodelet, J. P. *Electrochem. Commun.* **2009**, *11*,

1986–1989. (c) Gang, W.; More, K. L.; Johnston, C. M.; Zelenay, P. *Science (Washington, DC, U.S.)* **2011**, *332*. (d) Piana, M.; Catanorchi, S.; Gasteiger, H. A. *Electrochem. Soc. Trans.* **2008**, *16*, 2045–2055.

(5) (a) Meadowcr, D. *Nature* **1970**, *226*, 847. (b) Suntivich, J.; Gasteiger, H. A.; Yabuuchi, N.; Nakanishi, H.; Goodenough, J. B.; Shan-Horn, Y. *Nat. Chem.* **2011**, *3*, 546–550.

(6) (a) Sugawara, M.; Ohno, M.; Matsuki, K. *J. Mater. Chem.* **1997**, *7*, 833–836. (b) Cheng, F.; Shen, J.; Peng, B.; Pan, Y.; Tao, Z.; Chen, J. *Nat. Chem.* **2011**, *3*, 79–84.

(7) (a) Gong, K.; Du, F.; Xia, Z.; Durstock, M.; Dai, L. *Science (Washington, DC, U.S.)* **2009**, *323*, 760–764. (b) Liu, R.; Wu, D.; Feng, X.; Muellen, K. *Angew. Chem., Int. Ed.* **2010**, *49*, 2565–2569. (c) Su, D. S.; Zhang, J.; Frank, B.; Thomas, A.; Wang, X.; Paraknowitsch, J.; Schloegl, R. *ChemSusChem* **2010**, *3*, 169–180.

(8) (a) Guo, S. J.; Dong, S. J. *Chem. Soc. Rev.* **2011**, *40*, 2644–2672. (b) Sgobba, V.; Guldi, D. M. *Chem. Soc. Rev.* **2009**, *38*, 165–184. (c) Eder, D. *Chem. Rev.* **2010**, *110*, 1348–1385.

(9) Lota, G.; Fic, K.; Frackowiak, E. *Energy Environ. Sci.* **2011**, *4*, 1592–1605.

(10) (a) Seger, B.; Kamat, P. V. *J. Phys. Chem. C* **2009**, *113*, 7990–7995. (b) Park, S.; Shao, Y. Y.; Wan, H. Y.; Rieke, P. C.; Viswanathan, V. V.; Towne, S. A.; Saraf, L. V.; Liu, J.; Lin, Y. H.; Wang, Y. *Electrochem. Commun.* **2011**, *13*, 258–261. (c) Tang, H.; Chen, J. H.; Huang, Z. P.; Wang, D. Z.; Ren, Z. F.; Nie, L. H.; Kuang, Y. F.; Yao, S. Z. *Carbon* **2004**, *42*, 191–197. (d) Guo, S.; Sun, S. *J. Am. Chem. Soc.* **2012**, *134*, 2492–2495.

(11) Liang, Y.; Li, Y.; Wang, H.; Zhou, J.; Wang, J.; Regier, T.; Dai, H. *Nat. Mater.* **2011**, *10*, 780–786.

(12) Liang, Y.; Wang, H.; Zhou, J.; Li, Y.; Wang, J.; Regier, T.; Dai, H. *J. Am. Chem. Soc.* **2012**, *134*, 3517–3523.

(13) Wang, H.; Liang, Y.; Li, Y.; Dai, H. *Angew. Chem., Int. Ed.* **2011**, *50*, 10969–10972.

(14) Li, Y.; Zhou, W.; Wang, H.; Xie, L.; Liang, Y.; Wei, F.; Idrobo, J.-C.; Pennycook, S. J.; Dai, H. *Nat. Nano* **2012**, *7*, 394–400.

(15) Georgakilas, V.; Gournis, D.; Tzitzios, V.; Pasquato, L.; Guldi, D. M.; Prato, M. *J. Mater. Chem.* **2007**, *17*, 2679–2694.

(16) Liu, J.; Rinzler, A. G.; Dai, H. J.; Hafner, J. H.; Bradley, R. K.; Boul, P. J.; Lu, A.; Iverson, T.; Shelimov, K.; Huffman, C. B.; Rodriguez-Macias, F.; Shon, Y. S.; Lee, T. R.; Colbert, D. T.; Smalley, R. E. *Science (Washington, DC, U.S.)* **1998**, *280*, 1253–1256.

(17) Holzinger, M.; Vostrowsky, O.; Hirsch, A.; Hennrich, F.; Kappes, M.; Weiss, R.; Jellen, F. *Angew. Chem., Int. Ed.* **2001**, *40*, 4002.

(18) Bahr, J. L.; Yang, J. P.; Kosynkin, D. V.; Bronikowski, M. J.; Smalley, R. E.; Tour, J. M. *J. Am. Chem. Soc.* **2001**, *123*, 6536–6542.

(19) Han, W. Q.; Zettl, A. *Nano Lett.* **2003**, *3*, 681–683.

(20) Park, J. H.; Ko, J. M.; Park, O. O. *J. Electrochem. Soc.* **2003**, *150*, A864–A867.

(21) Shan, Y.; Gao, L. *Chem. Lett.* **2004**, *33*, 1560–1561.

(22) Hummers, W. S.; Offeman, R. E. *J. Am. Chem. Soc.* **1958**, *80*, 1339–1339.

(23) Wang, H.; Casalongue, H. S.; Liang, Y.; Dai, H. *J. Am. Chem. Soc.* **2010**, *132*, 7472–7477.

(24) Casella, I. G.; Gatta, M. *J. Electroanal. Chem.* **2002**, *534*, 31–38.

(25) De Koninck, M.; Poirier, S.-C.; Marsan, B. *J. Electrochem. Soc.* **2006**, *153*, A2103–A2110.

(26) Xu, J.; Gao, P.; Zhao, T. S. *Energy Environ. Sci.* **2012**, *5*, 5333–5339.

(27) Zheng, F.; Alayoglu, S.; Guo, J.; Pushkarev, V.; Li, Y.; Glans, P.-A.; Chen, J.-I.; Somorjai, G. *Nano Lett.* **2011**, *11*, 847–853.

(28) Morales, F.; de Groot, F. M. F.; Glatzel, P.; Kleimenov, E.; Bluhm, H.; Havecker, M.; Knop-Gericke, A.; Weckhuysen, B. M. J. *Phys. Chem. B* **2004**, *108*, 16201–16207.

(29) Abbate, M.; Goedkoop, J. B.; Degroot, F. M. F.; Griioni, M.; Fuggle, J. C.; Hofmann, S.; Petersen, H.; Sacchi, M. *Surf. Interface Anal.* **1992**, *18*, 65–69.

(30) (a) Zhou, J.; Wang, J.; Fang, H.; Sham, T.-K. *J. Mater. Chem.* **2011**, *21*, 5944–5949. (b) Zhang, L.-S.; Liang, X.-Q.; Song, W.-G.; Wu, Z.-Y. *Phys. Chem. Chem. Phys.* **2010**, *12*, 12055–12059.

(31) Zhou, J. G.; Fang, H. T.; Hu, Y. F.; Sham, T. K.; Wu, C. X.; Liu, M.; Li, F. J. *Phys. Chem. C* **2009**, *113*, 10747–10750.

(32) (a) Bezerra, C. W. B.; Zhang, L.; Lee, K.; Liu, H.; Marques, A. L. B.; Marques, E. P.; Wang, H.; Zhang, J. *Electrochim. Acta* **2008**, *53*, 4937–4951. (b) Jaouen, F.; Proietti, E.; Lefevre, M.; Chenitz, R.; Dodelet, J.-P.; Wu, G.; Chung, H. T.; Johnston, C. M.; Zelenay, P. *Energy Environ. Sci.* **2011**, *4*, 114–130. (c) Morozan, A.; Jegou, P.; Josselme, B.; Palacin, S. *Phys. Chem. Chem. Phys.* **2011**, *13*, 21600–21607.

(33) Paulus, U. A.; Schmidt, T. J.; Gasteiger, H. A.; Behm, R. J. *J. Electroanal. Chem.* **2001**, *495*, 134–145.